DD

ISTITUTO NAZIONALE DI FISICA NUCLEARE

Sezione di Trieste

SW9632

A. Rashevsky, V. Bonvicini, P. Burger, L. Vinogradov, A. Vacchi and N. Zampa

NEW DEVELOPMENTS IN SILICON DRIFT DETECTORS

NEW DEVELOPMENTS IN
SILICON DRIFT DETECTORS

A. Rashevsky[1], V. Bonvicini[1], P. Burger[3],

L. Vinogradov[1,2], A. Vacchi[1] and N. Zampa[1]

1 Dipartimento di Fisica dell'Università di Trieste, Italy and INFN, Sezione di Trieste, Italy

2 University of Saint Petersburg , Russia

3 Canberra Semiconductor, NV 2250 Olen, Belgium

Abstract

In the frame of the INFN DSI project (development of large area linear drift detectors) several prototypes have been designed and produced. The function of these prototypes is to allow the evaluation of the solutions chosen for the geometry of the on board electrodes and the production process. On these prototypes we have studied the static characteristics and measured time-of-flight and charge collection injecting charges with an IR laser source.

1. Introduction

Silicon drift detectors (SDD) are depleted by inversely biasing the detector through the p^+ structures on both faces and a small n^+ collection anode [1÷7]. This greatly reduces the collection electrode capacitance hence the energy resolution limit. By measuring the drift time of the signal electrons to the readout anodes a good position resolution (10÷20 µm) is obtained unambiguously for the two co-ordinates. Compared to both strip and pixel detectors the SDD has a small number

1

of readout channels offering meanwhile a good energy resolution and high granularity pixel-like position measurements. The SDD is well suited for track detection in high energy physics especially in presence of high particle density. The use of SDD in a real experiment still requires to reach effective production of large area high quality detectors. The aim of our work is to establish a manufacturing process and a detector geometry which will facilitate the use of the drift chamber concept with all its advantages in a wide field of applications.

2. The prototypes

Seven different test structures were designed to be realised on 4" diameter wafers of neutron transmutation doped (NTD) silicon with resistivity of 3000 Ohm cm. All basic elements implemented in the prototypes such as drift electrodes, high voltage divider, guard electrode structure, charge injection electrodes and charge collection zone were first carefully simulated [8]. The largest number of geometry variations was introduced for the on board high voltage divider. The drift length in each of the prototypes is 16 mm while the sensitive area is 2 cm^2 for the one-directional structures and twice as much for the "butterfly" bi-directional structures. The array of anodes with 200 μm pitch collects the drifting charges. Most of the structure of the cathodes has a pitch of 120 μm with a gap between p$^+$-implants of 50 μm. In some structures the metal extends 5 μm beyond the p$^+$-implants in order to smoothen the electric field at the most stressed edges of the drift electrodes. To set the optimal collection field in the region of the anodes, a few cathodes next to the anodes are externally biased. The details of one of the "butterfly" prototypes relevant to the results presented here are shown in Fig.1a,b.

3. Experimental set-up

To perform electrical measurements on the available prototypes as well as time-of-flight measurements, we have realized a modular printed circuit board (PCB). The test structures were mounted on detector cards, which in their turn could be plugged into a motherboard. The front end electronics, the high and low bias voltages, as well as checkpoints for the static electrical measurements, were placed on the motherboard while all necessary bondings to the structure were made at the level of the detector card. Few hours are enough to prepare and test a new detector.

Three power supplies were used: one to bias the integrated high voltage divider of the drift structure (with capability to monitor the current through the divider), one to bias the drift electrodes in the collection region close to the anodes, through external voltage dividers, and a third one for the front end electronics.

For drift time measurements we used the following apparatus. The PCB and one of the detector cards were fixed on a XY micrometric stage having a position resolution of ±1 μm for both axes. A focused IR laser mounted on an optical stage was used to inject charge into the drift detector. The wavelength of the laser was 850 nm. The light pulse duration was less than 50 ps. The repetition time was 100 μs with jitter less than ±10 ps (as declared in the laser specifications). The number of electrons generated in the detector was maximal when the laser spotlight was placed in a gap between two drift electrodes and minimal when it was on the drift electrode covered with metallization. Thus, going across the drift electrodes with the spotlight, one could observe the induced pulse height modulation of the signal at the anodes. We measured the dependence of the pulse height versus the position of the spotlight (Fig.2). When the spotlight is in the gap of 40 μm between drift electrodes the pulse height remains constant for at least 5 μm. From this we concluded that all the light is contained in a spot with 35 μm diameter.

The front end electronics consists of a commercial charge-sensitive hybrid preamplifier and hybrid bipolar shaper with a peaking time of 180 ns. The output voltage corresponding to the charge deposited by a minimum ionizing particle (m.i.p.) in 300 μm of silicon (3.84 fC) was 23 mV. The number of electrons generated in the detector during one laser pulse was equivalent to the charge produced by 50 m.i.p. To measure precisely the drift times we used a DAQ system consisting of flash ADCs communicating through VME/VMV bus with a MAC Q700 computer. A schematic block-diagram of the set-up is shown in Fig.3. The flash ADCs STR755 belong to the STRUCK750 system and are driven by the master unit STR751 [9]. Each STR755 ADC has 8 channels with 8 bit linear resolution and 2048 byte ring memory. The system has an internal clock generator with a frequency of 40 MHz, which is in common to all ADCs, so that the sampling period is 25 ns. Since the clock generator is a free-running oscillator there is a jitter of 25 ns in the start of conversion. We sent to one of the channels of the flash ADCs the trigger signal delayed by a short time (about 90 ns). By subtracting the reading of this reference channel from all others we got rid of this jitter uncertainty. Neglecting the front end electronics and external pick-up noise, the intrinsic error of this system in the measurement of the drift time is determined by two factors: 1) the pulse height of the signal from an anode as soon as there is an uncertainty of $\pm 1/2$ LSB (least significant bit) in analogue-to-digit conversion, and 2) the number of samplings used to digitise a signal. The influence of these two factors on the time resolution is illustrated in Fig.4. As one can see at any given pulse height these two factors are contrary to each other: while the higher number of samplings tends to improve the time resolution, the higher number of analogue-to-digit conversions tends to decrease it. With a shaper peaking time of 180 ns the signal was sampled 14 times, while the pulse height varied from 100 to 50 channels of the flash ADC depending on the drift distance and drift field (it will be discussed later). We have used a software developed in the frame of LabVIEW® [10], which allowed to analyse time and amplitude information in a multichannel regime.

4

4. Results

Thinking to the use of large amounts of detectors, it is important to reduce the production costs and increase the yield. The solution of the production problems is correlated to the structures of the device and their simplicity. To enlarge the reliability of the detectors we have put a lot of care in reducing the field strengths on the edges of the electrodes. The drift electrodes have been designed to be operated at high drift field [8]. Indeed, it was possible to operate the tested drift detectors up to the highest field made available by the HV power supply (700 V/cm). Also the guard structure at the edge of the detector was designed to withstand high drift field as soon as guard strips connect every second drift electrode and the potential difference between contiguous guard strips is twice as much as between drift ones. In order to determine the maximal drift field which is possible to create in the available prototype detectors before the punch through effect happens we measured the current between contiguous guard strips as a function of voltage between them (Fig.5). The punch through effect starts at the voltage higher than 26 V. This voltage corresponds to the drift field of 1080 V/cm. The results we obtained from the on board divider show its linear behaviour. In Fig.6a we report the measured potential distributions on the drift electrodes. Both dividers (n-side and p-side of the detector) are pretty linear and the potential distributions practically coincide at all applied bias voltages. At the bias voltage of -1024 V, which corresponds to a drift field of 670 V/cm, the standard deviations of the measured points from the 'ideal' potential distribution at the high voltage divider are 0.7 V and 0.4 V for n-side and p-side respectively (Fig.6b). Fig.7 presents the linear fit of the total divider current versus the bias voltage. The divider resistivity of 77 kΩ/gap calculated from this fit is in a good agreement with the designed value. In Fig.8a we report the drift time versus drift distance distributions for three different drift fields. The recalculated mobility value showed some consistent change with the drift field induced by the

5

different power dissipation at different values of the current flowing through the integrated voltage divider. Deviation of the drift time from the linear fit for the drift field of 700 V/cm is shown in Fig.8b and the standard deviation σ is 2.1 ns. Points in the collection zone which starts at 0.8 mm distance from the anodes were not included in the linear fit. All points of the drift time versus distance plots (Fig.8a) were measured at high statistics in order to determine the standard deviation from the mean value for each individual point (Fig.9a). The measurements were done at the drift field of 700 V/cm. When the laser spotlight is positioned close to anodes (the upper plot) the drift time distribution is mainly determined by the finite size of the spotlight and by the front end electronics and external pick-up noise. The standard deviation σ_0 of this 'reference' distribution is 1.8 ns. With the spotlight going further from anodes the drift time distribution gets wider due to the influence brought by the detector itself. Thus we can define the detector contribution to the standard deviation σ in the drift time distribution as $(\sigma_{detector})^2 = \sigma^2 - (\sigma_0)^2$. At the drift distance of 15.2 mm, that is almost in the middle of the bi-directional detector (the longest drift distance is 16.3 mm), $\sigma_{detector} = 2.1$ ns. At the drift field of 700 V/cm the drift velocity v_{drift} is 8 μm/ns, hence we can declare the position resolution of the prototype detector as $\sigma_{position} = v_{drift} \times \sigma_{detector} = 17$ μm. Fig.9b presents $\sigma_{position}$ as a function of the drift distance. At the drift field of 700 V/cm we performed a careful scanning of the whole sensitive zone. We measured 18 distributions of the drift time versus drift distance, going with a step of 0.8 mm along the axis parallel to the anodes. In this way all the sensitive zone was covered with a matrix of measurements, including also the parts occupied with the divider embedded into the drift electrodes. Then a linear fit was done, taking into account all these measurements. Standard deviation of the measured points from the linear fit is 1.7 ns, which being multiplied with the drift velocity gives 13.5 μm. Rather good uniformity of drift in different parts of the sensitive area is illustrated in Fig.10a,b,c where at three different drift distances the drift time is presented as a function of the position on the axis parallel to the anodes. The zero of the axis

corresponds to the median of the anode array. One can notice the values at the flanks of the distribution are not much different than in the centre, this even in the presence of the integrated voltage divider at the flanks of the sensitive zone.

To measure the charge collection efficiency we connected 36 anodes to one readout channel and positioned the laser spotlight at two extreme points of the sensitive drift zone: at the beginning (1 mm from the anodes) and at the very edge of (16 mm from the anodes). We analized both the height of the pulse and its area, increasing the drift field. From the plots presented in Fig.11a one can see two features: first, the dependence of the charge collection efficiency on the drift field, that is on the drift time, and, second, the difference in efficiencies obtained from the pulse height and pulse area measurements. We explain it by the effect of diffusion and electrostatic repulsion of the initially compact electron cloud during its drift towards the anodes [11]. This effect induces the amplitude ballistic deficit of the front end electronics, as well as the apparent charge loss, when some part of the drift electrons successfully arrived to the anodes are not read out because the preamplifier rise time is less than the time duration of the electron cloud. In comparison with the pulse height measurements the pulse area measurements are less dependent on this effect, though they still do not reflect entirely the real share of drift electrons which have reached the anodes. To prove it we investigated the response of the front end electronics to test pulses imitating the signal charge at the preamplifier input. With 36 anodes connected together to the preamplifier input the measured rise time of the preamplifier was 190 ns. Varying the input pulse duration from 20 ns to 600 ns we measured the shaper pulse area. Data were normalized to the value measured at the imitating pulse duration of 20 ns. From the charge collection efficiency measurements described above we knew the experimental values of the drift time, so it was possible to recalculate the time duration of the electron cloud affected by the diffusion and electrostatic repulsion [11]. Both sets of the data are presented in Fig.11b. One can see the change of slope in the curve 'b' around the value of 190 ns. This can be explained by the fact that up to the value of

7

the preamplifier rise time only the ballistic deficit plays a role, while for a longer pulse duration the output signal is limited also by the preamplifier rise time. It is clear that the dependence of the charge collection efficiency on the electric field is mainly determined by the preamplifier rise time. One should take in mind that we worked with rather large number of electrons generated in the detector by the laser and the charge produced by one m.i.p. would be less affected by the electrostatic repulsion, resulting in a higher charge collection efficiency.

5. Future developments

The results obtained on the prototype detectors demonstrated the stability and high quality performances of SDD. The next step is the production of a detector with larger sensitive area and with an optimised sensitive-to-total area ratio. The design of this detector is now completed and the production run is to be finished in the summer of 1996. The new detector has a total area of 8.00×6.75 cm^2 with a sensitive-to-total area ratio of 86%. It is a "butterfly" bi-directional detector with 384 anodes on both sides. A dedicated VLSI front end electronics was realised using a full-custom, bipolar process by Tektronix [12]. The cell features 32 channels, each one comprising a charge preamplifier, a semi-gaussian shaper and a symmetrical line driver. The cell has a shaping time of 55 ns and ENC at 0 pF load is 250 e^- RMS. The cell gain is 30 mV/fC.

6. Acknowledgements

References

[1] E. Gatti and P. Rehak, Nucl. Instr. and Meth. **A225** (1984) 608.

[2] P. Rehak et al Nucl. Instr. and Meth. **A248** (1986) 367.

[3] E. Gatti, P. Rehak, and J.T. Walton, Nul. Instr. and Meth. **A226** (1984) 129.

[4] J. Kemmer, Nucl. Instrum. and Meth. **A226**, (1984) 89.

[5] E. Gatti, A. Longoni, M. Sampietro, P. Giacomelli, P. Rehak, J. Kemmer, W. Kubishta, P. Holl, L. Struder, and A. Vacchi,

Nucl. Instr. and Meth. **A273**, 865 (1988).

[6] E. Gatti, A. Castoldi, S. Chinnici, A. Longoni, F. Palma, P. Rehak, M. Sampietro and A. Vacchi, Nucl. Instr. and Meth. **A306** (1991) 187.

[7] E. Gatti, A. Castoldi, A. Longoni, M. Sampietro, P. Rehak, and A. Vacchi, Nucl. Instr. and Meth. **A295** (1990) 4.

[8] G. Gramegna, E. Cantatore, F. Corsi, M. Cuomo, D. De Venuto, C. Marzocca, A. Vacchi, V. Manzari, F. Navach, S. Beole', G.Casse, P.Giubellino, L. Riccati, P. Burger. IEEE Trans. on Nuclear Science, vol.42, NO.5, October 1995.

[9] Company **Dr. Bernd Struck**, P.O.Box 1141, D-22886 Tangstedt, Germany

[10] LabVIEW® 3.2 (National Instruments®)

[11] E. Gatti, A. Longoni, P. Rehak and M. Sampietro, Nucl. Instr. and Meth. **A253** (1987) 393.

[12] W. Dabrowski, W. Bialas, G. Bonazzola, V. Bonvicini, F. Ceretto, P. Giubellino, M. Idzik, M. Prest, L. Riccati and N. Zampa.

Proceedings of the Villa Olmo Conference, Como, Oct. 1994

Figure captions

Fig.1a,b Details of the prototype structure.
1 - drift electrodes; 2 - resistors of the high voltage divider embedded in drift electrodes; 3 - guard electrodes; 4 - drift electrodes of collecting zone; 5 - collecting anodes; 6 - edge electrodes.

Fig.2 Pulse height of the signal at the anodes versus the position of the laser spotlight (1 μm per point). The drift electrode metallization (80 μm) and the gap between metallizations of the neighbouring drift electrodes (40 μm) are indicated as well as the drift direction.

Fig.3 Block-diagram of the experimental set-up.

Fig.4 Influence of the number of samplings and the pulse height on the time resolution of the acquisition system.

Fig.5 Current between contiguous guard strips versus the applied voltage.

Fig.6a Potential distribution measured at the drift electrodes of n-side and p-side of the prototype versus distance from the anodes.
Three pairs of curves correspond to four values of the drift field, from up down:
1) E = 167 V/cm; 3) E = 333 V/cm; 3) E = 667 V/cm.

Fig.6b Deviations of the potentials measured at the drift electrodes (1 out of 8 electrodes is accessible) from the 'ideal' potential distribution at the high voltage divider. Ubias = 1024 V which corresponds to the drift field of 667 V/cm. Squares and triangles indicate the deviation from a linear behaviour for n-side (anode side) and p-side dividers.

11

Fig.7 Total integrated divider current versus bias voltage.

Fig.8a Drift time versus distance from the anodes. Three distributions correspond to three values of the drift field:

squares: E = 200 V/cm; triangles: E = 400 V/cm; rhombuses: E = 700 V/cm.

Recalculated mobility values, respectively:

$\mu = 1397$ cm^2/V s; $\mu = 1306$ cm^2/V s; $\mu = 1145$ cm^2/V s.

Fig.8b Deviations from the linear fit interpolation of the time-of-flight distribution. Measurements were done at $U_{bias} = 1076$ V which corresponds to the drift field 700 V/cm.

Fig.9a Drift time distribution 'inside' individual points of the time-of-flight distribution (Fig.8a).

From up down:

a) 0.34 mm from anodes; standard deviation σ_0 is 1.8 ns,

b) 0.94 mm from anodes; standard deviation σ is 2.1 ns,

c) 5.62 mm from anodes; standard deviation σ is 2.4 ns,

d) 11.38 mm from anodes; standard deviation σ is 2.5 ns,

e) 15.22 mm from anodes; standard deviation σ is 2.8 ns.

Fig.9b Position resolution of the prototype detector $\sigma_{position}$ as a function of the drift distance.

Fig.10a,b,c Drift time as a function of the position on the axis parallel to the anodes. The zero of the axis corresponds to the median of the anode array. Dashed lines limit zones where the integrated divider is placed. Measurements were done at the drift field of 700 V/cm.

12

a) 5.62 mm from anodes,

b) 11.38 mm from anodes,

c) 15.22 mm from anodes.

Fig.11a Charge collection efficiency versus drift field. The laser spotlight was positioned at two extreme points of the sensitive drift zone: at the beginning (1 mm from the anodes) and the very edge (16 mm from the anodes). Both, the pulse height (squares) and area (triangles) of the signal were measured. Data are normalised on the maximum values corresponding to the laser spotlight positioned at 1 mm from the anodes.

Fig.11b Curve 'a' (rhombuses) - charge collection efficiency versus time duration of the electron cloud spread out due to the diffusion and electrostatic repulsion during the drift to the anodes; curve 'b' (squares) - shaper pulse area versus the duration of the generator current pulse imitating the drift electron cloud. Data are normalized on the shaper pulse area measured at the input pulse duration of 20 ns.
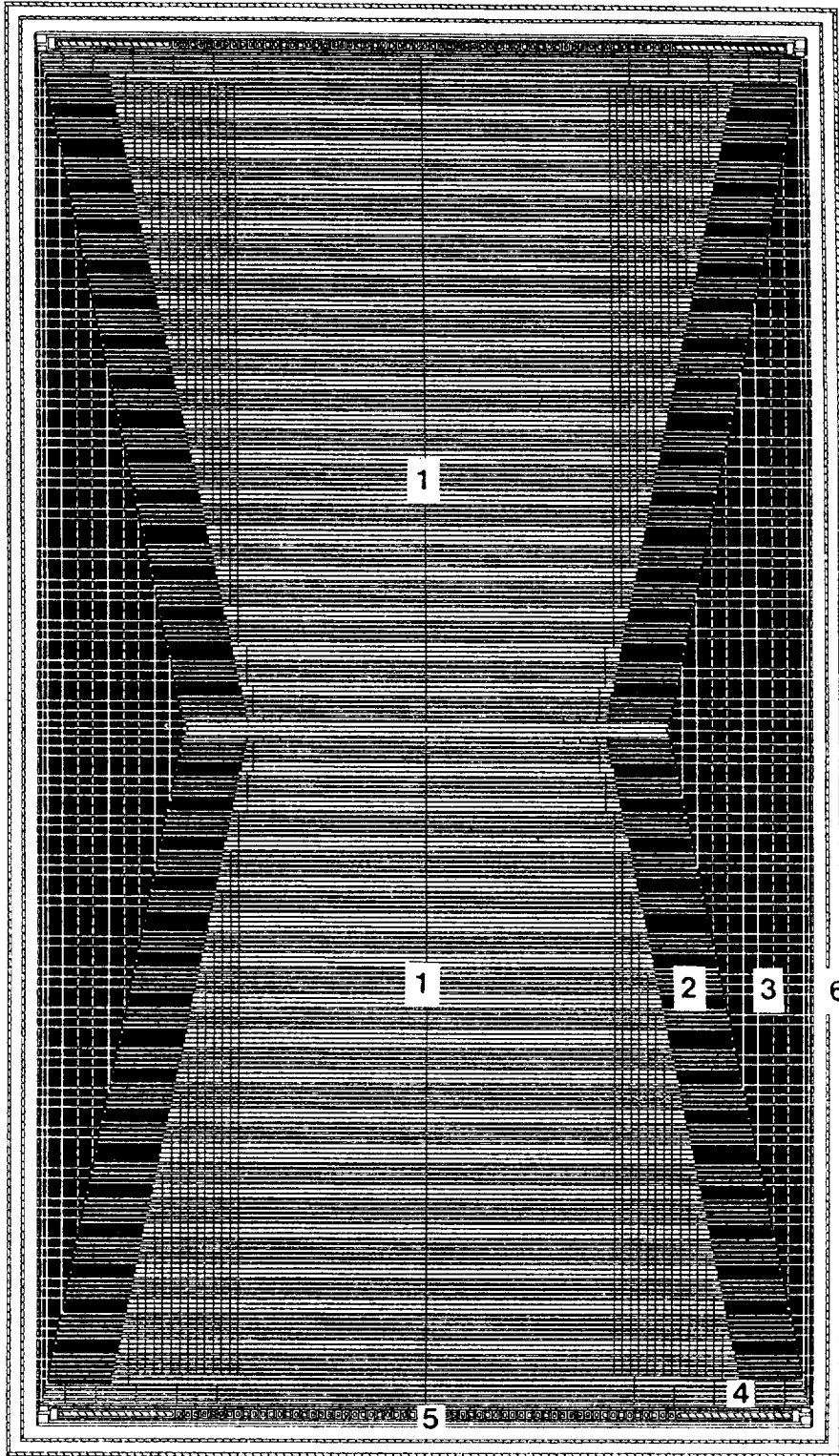
Fig. 1a
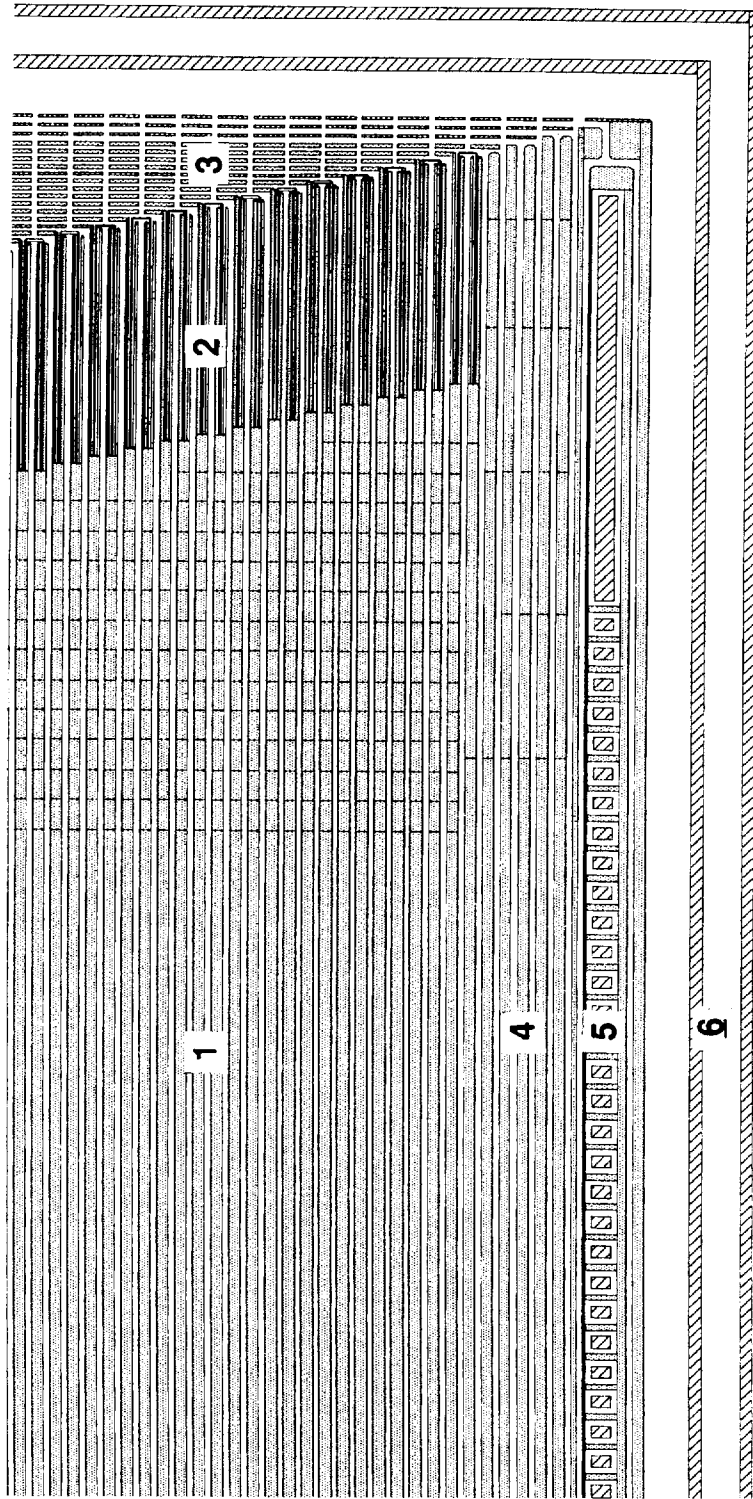
Fig. 1b
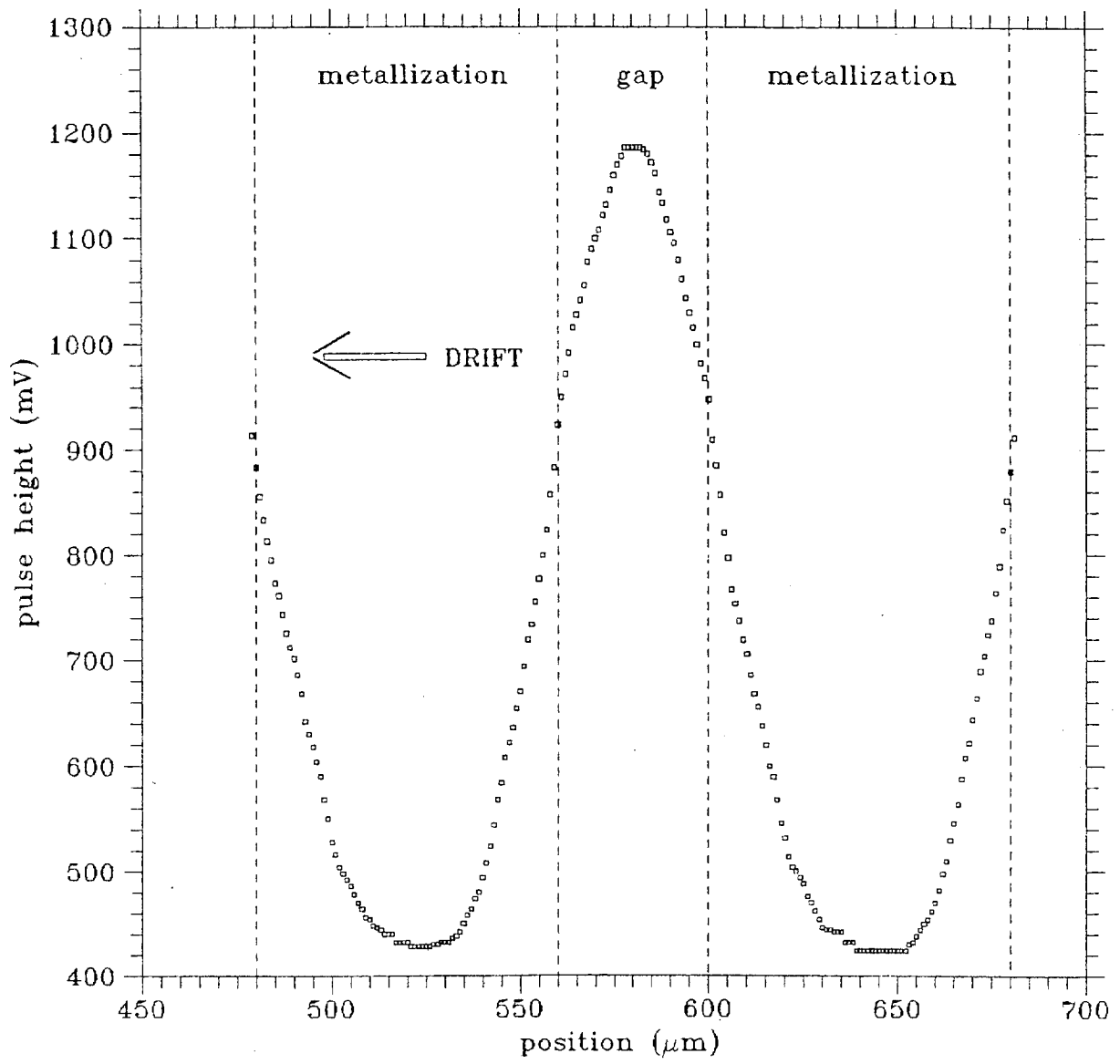
Fig. 2
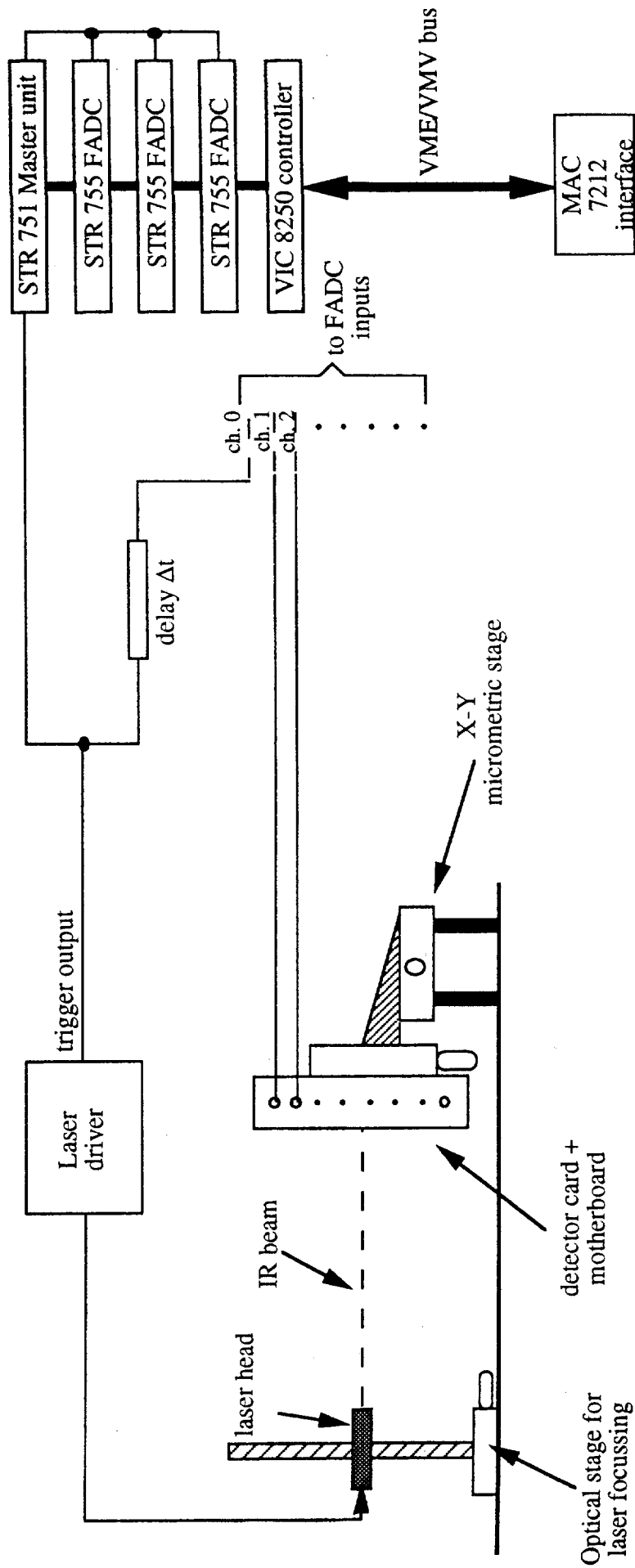
Fig. 3
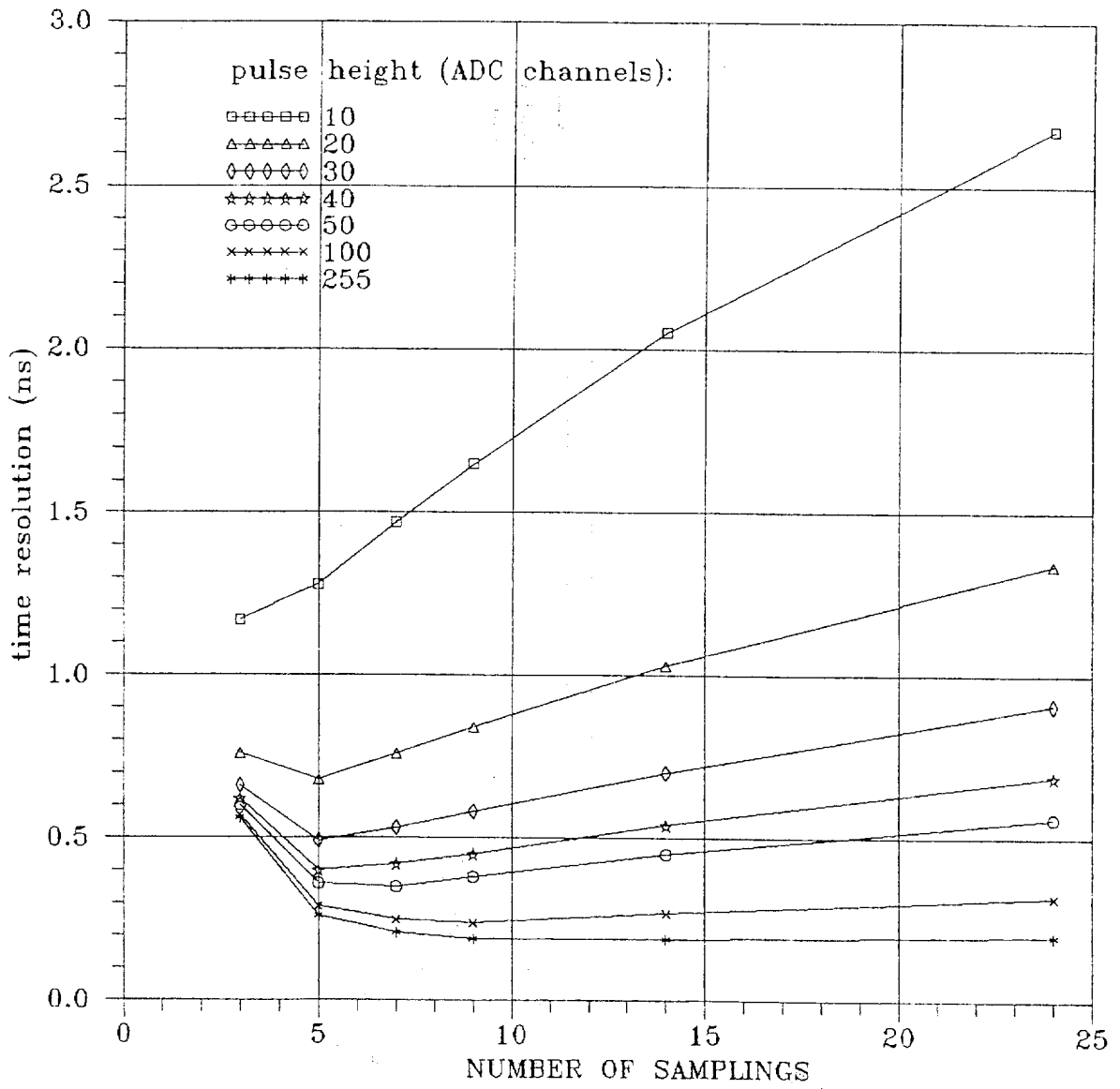
Fig. 4
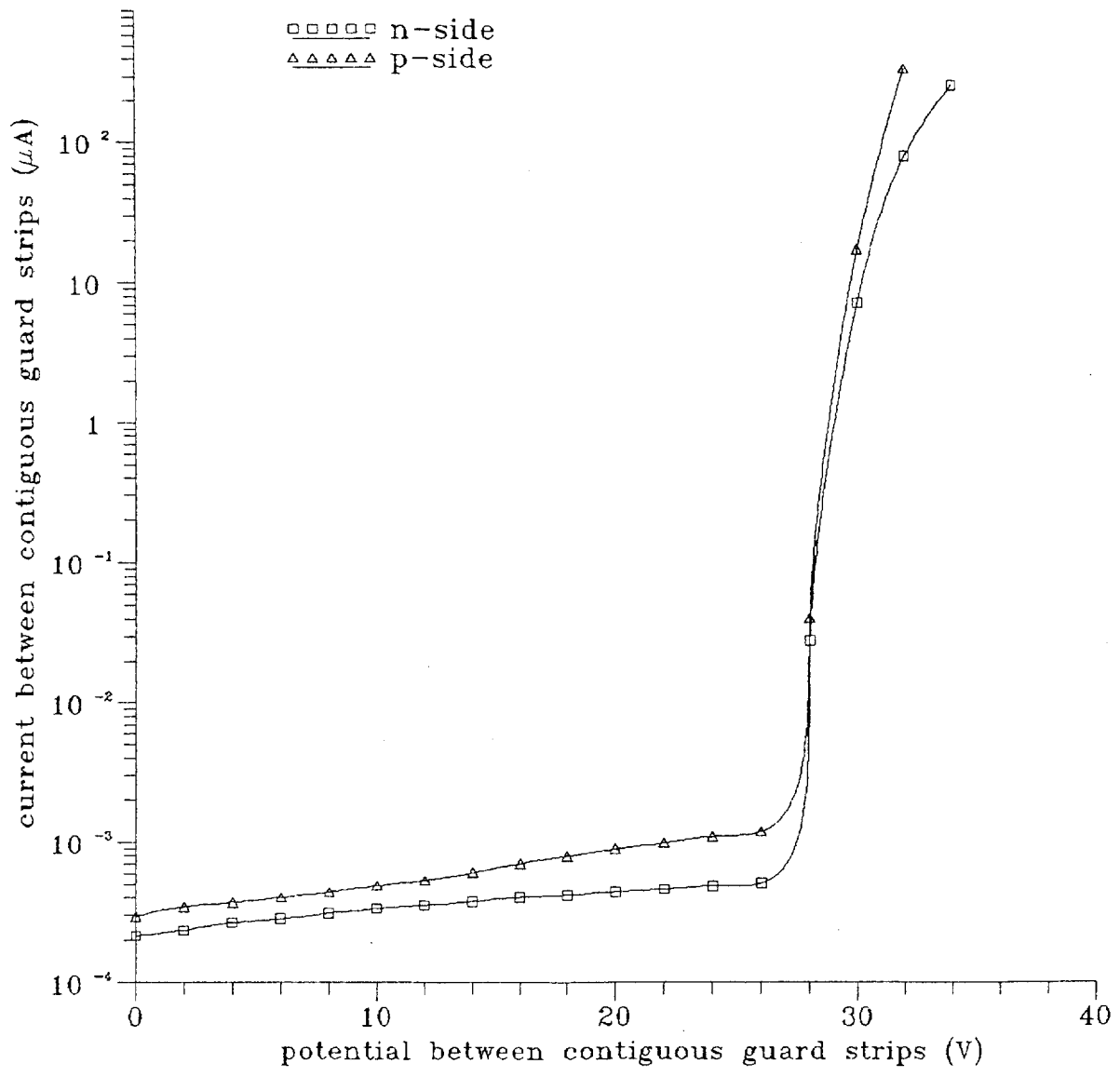
Fig. 5
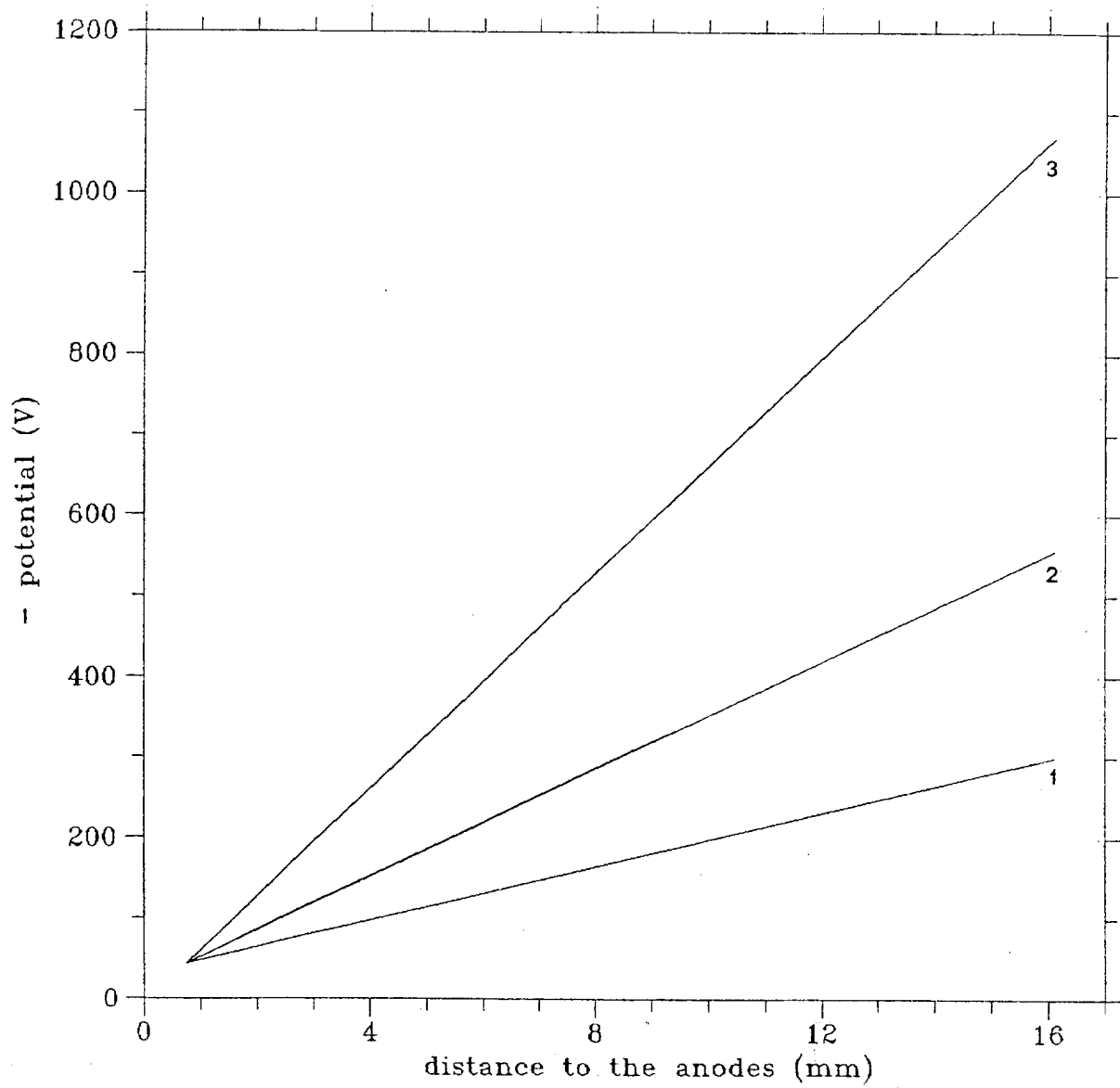
Fig. 6a
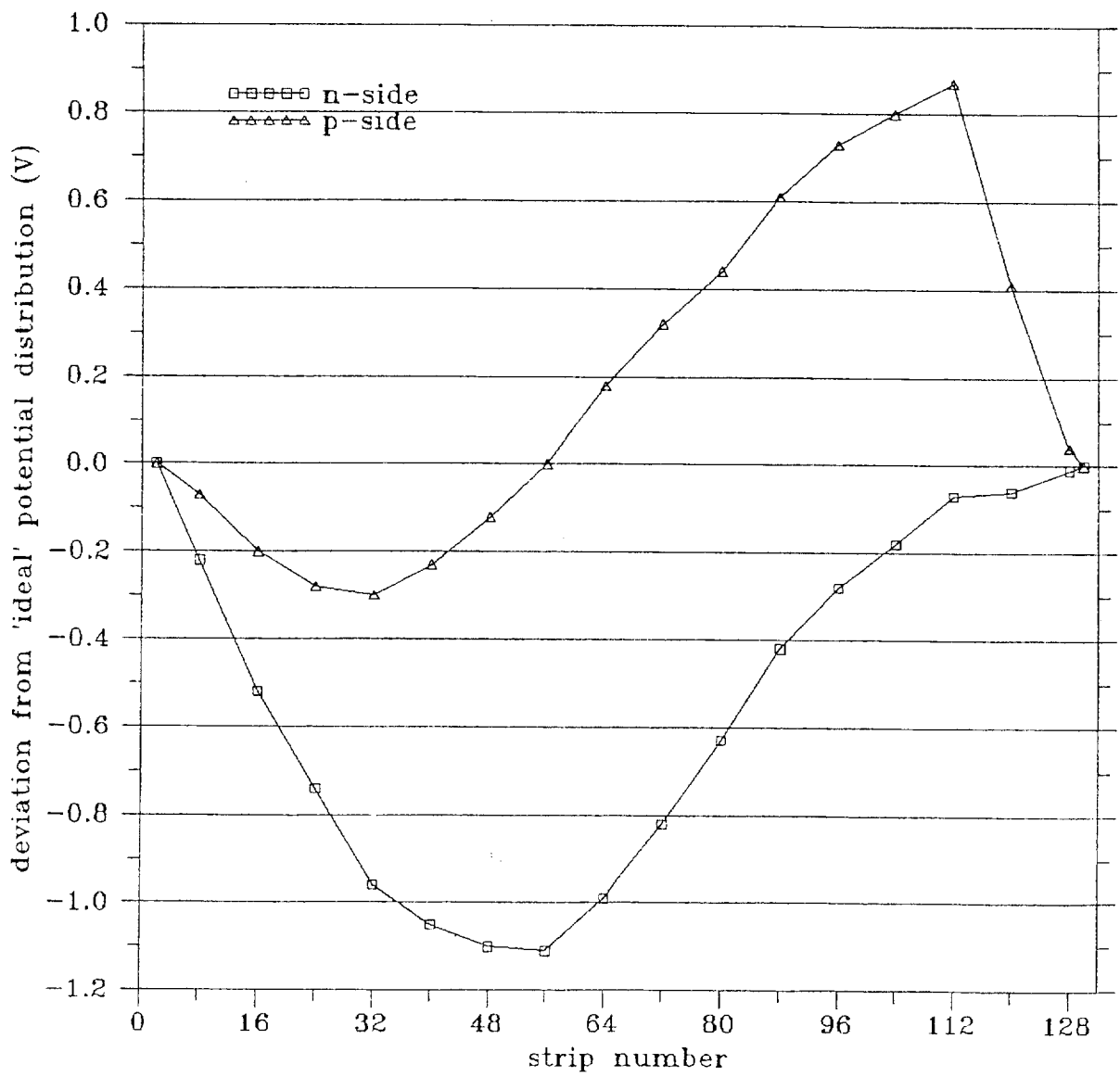
Fig. 6b

Fig. 7

Fig. 8a

Fig. 8b

events

drift time (ns ×0.25)
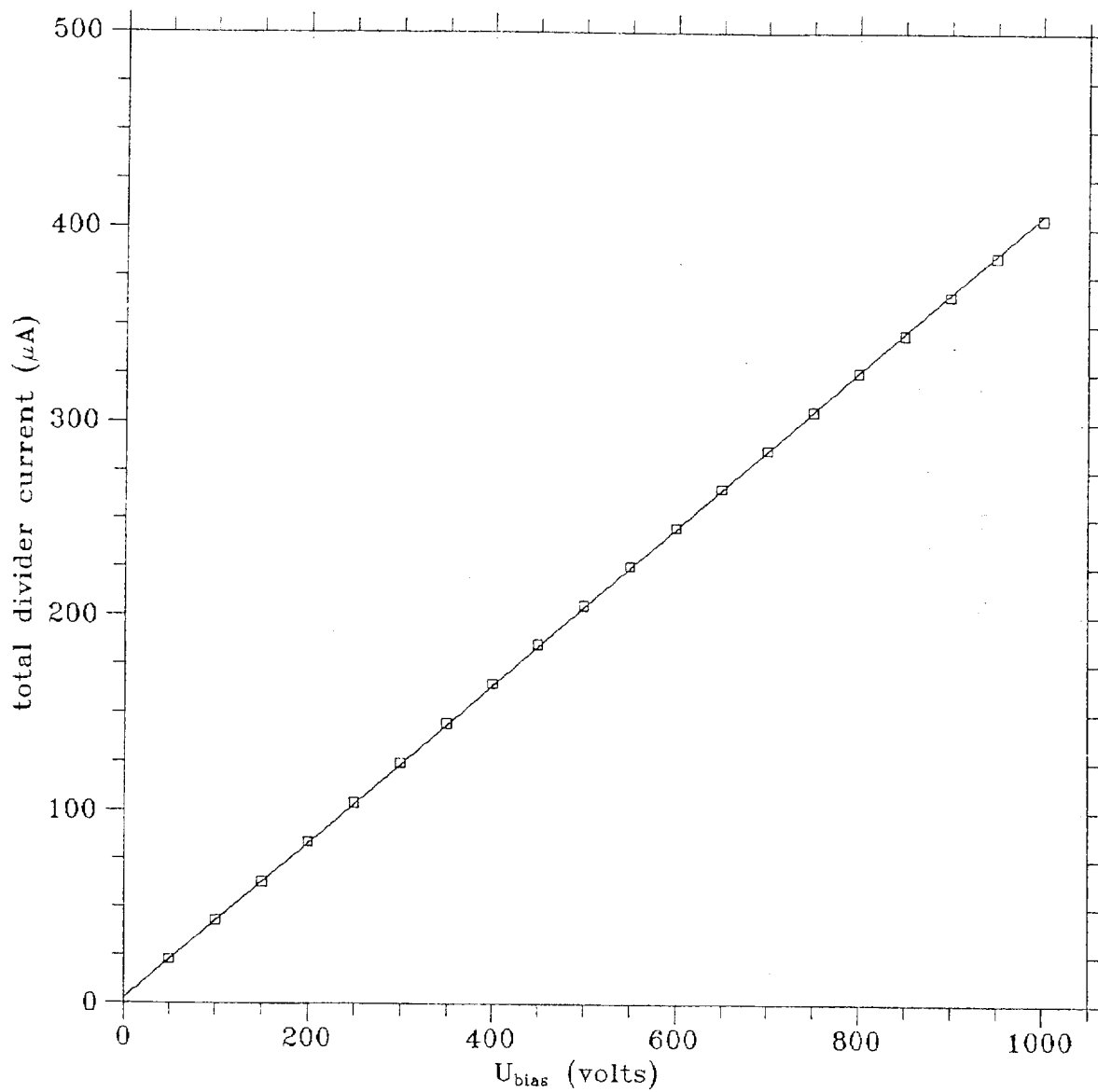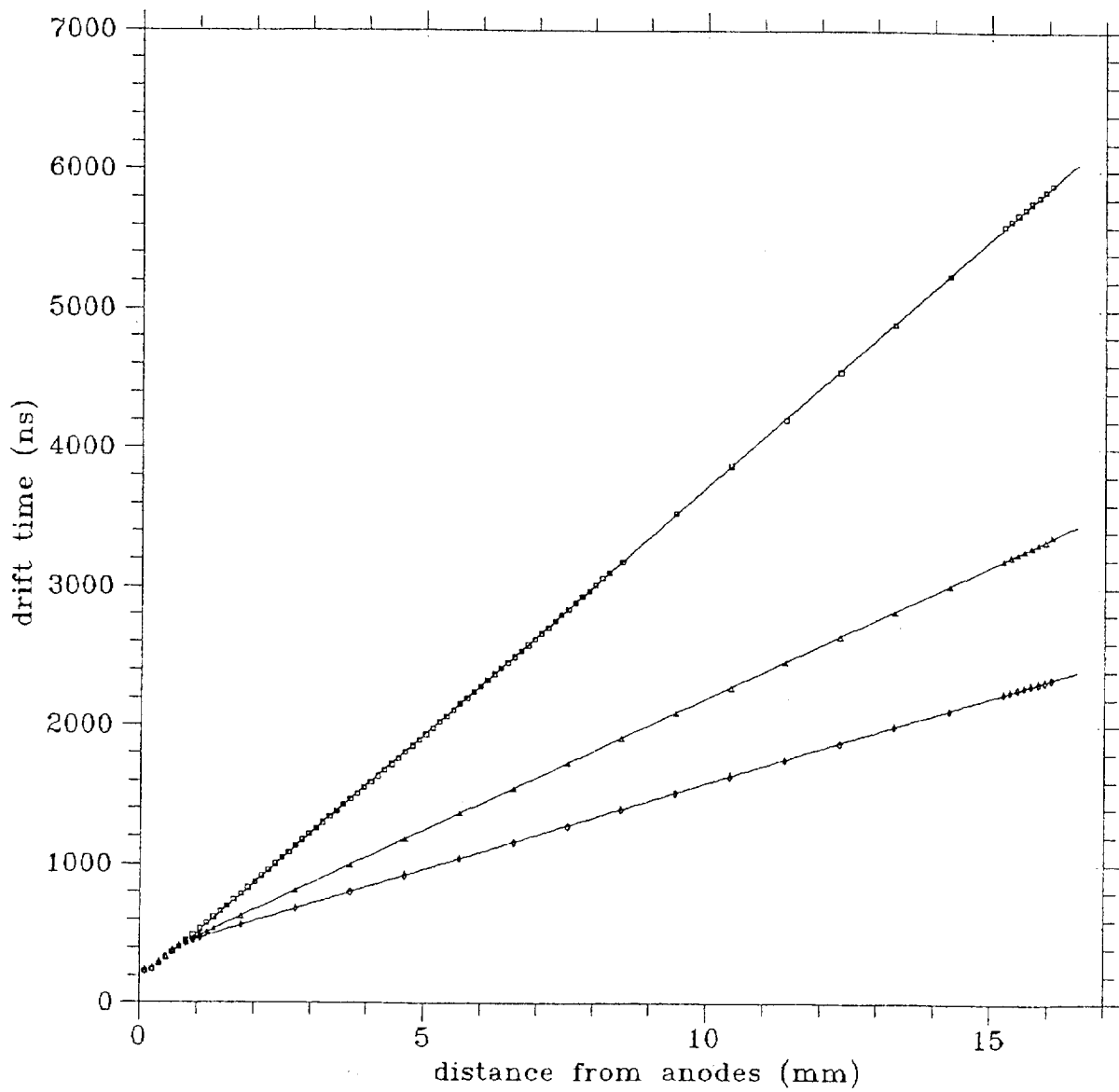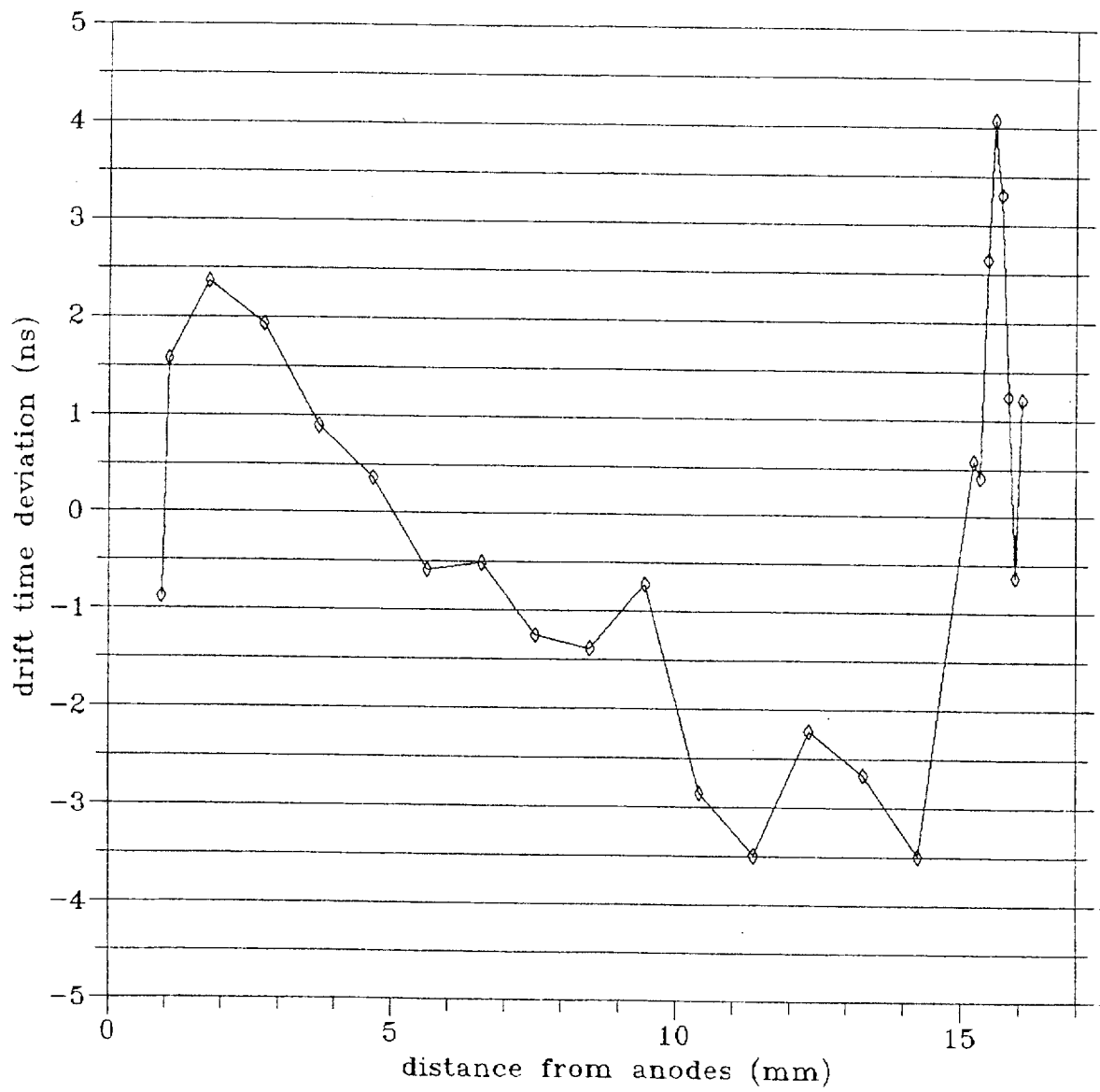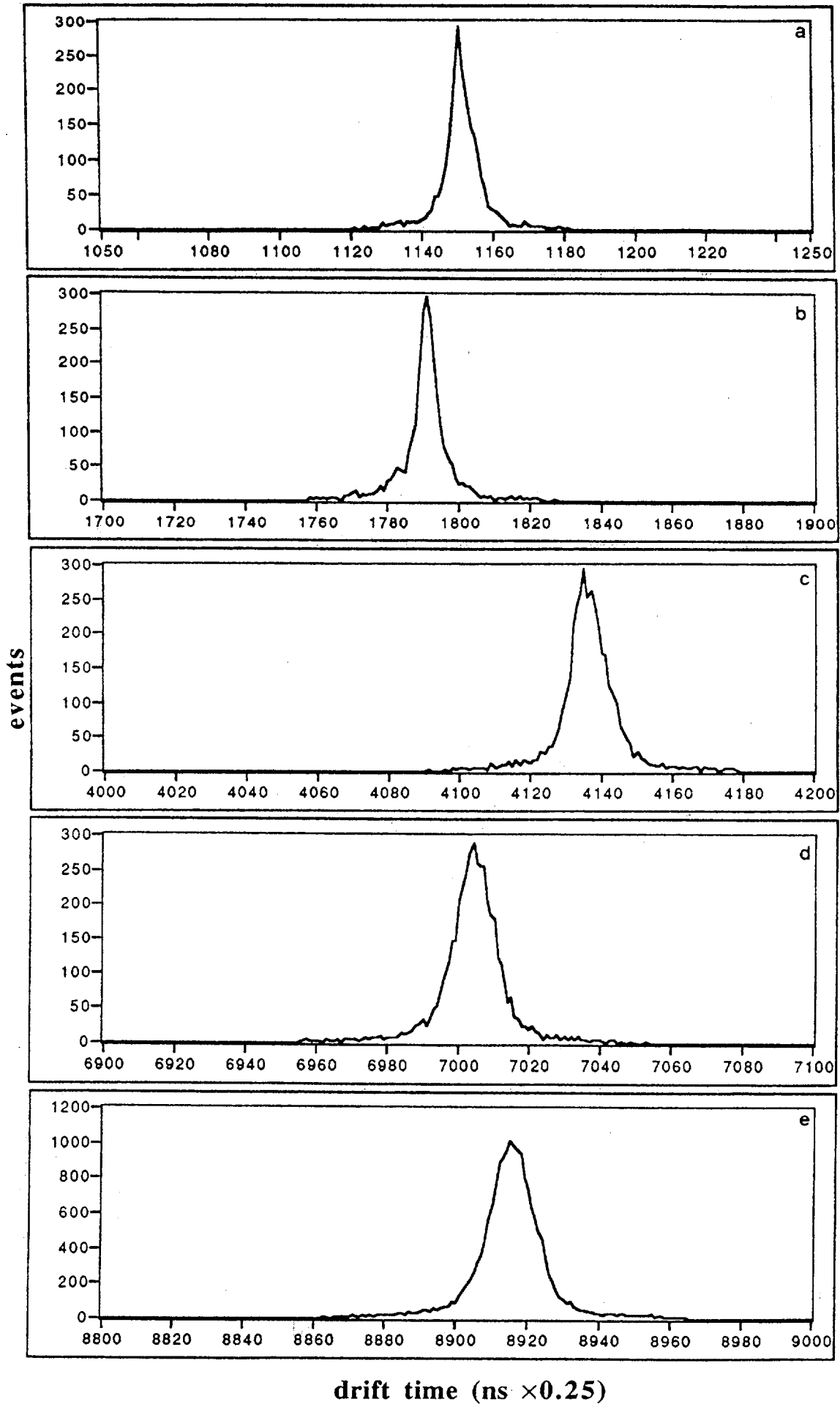
Fig. 9a
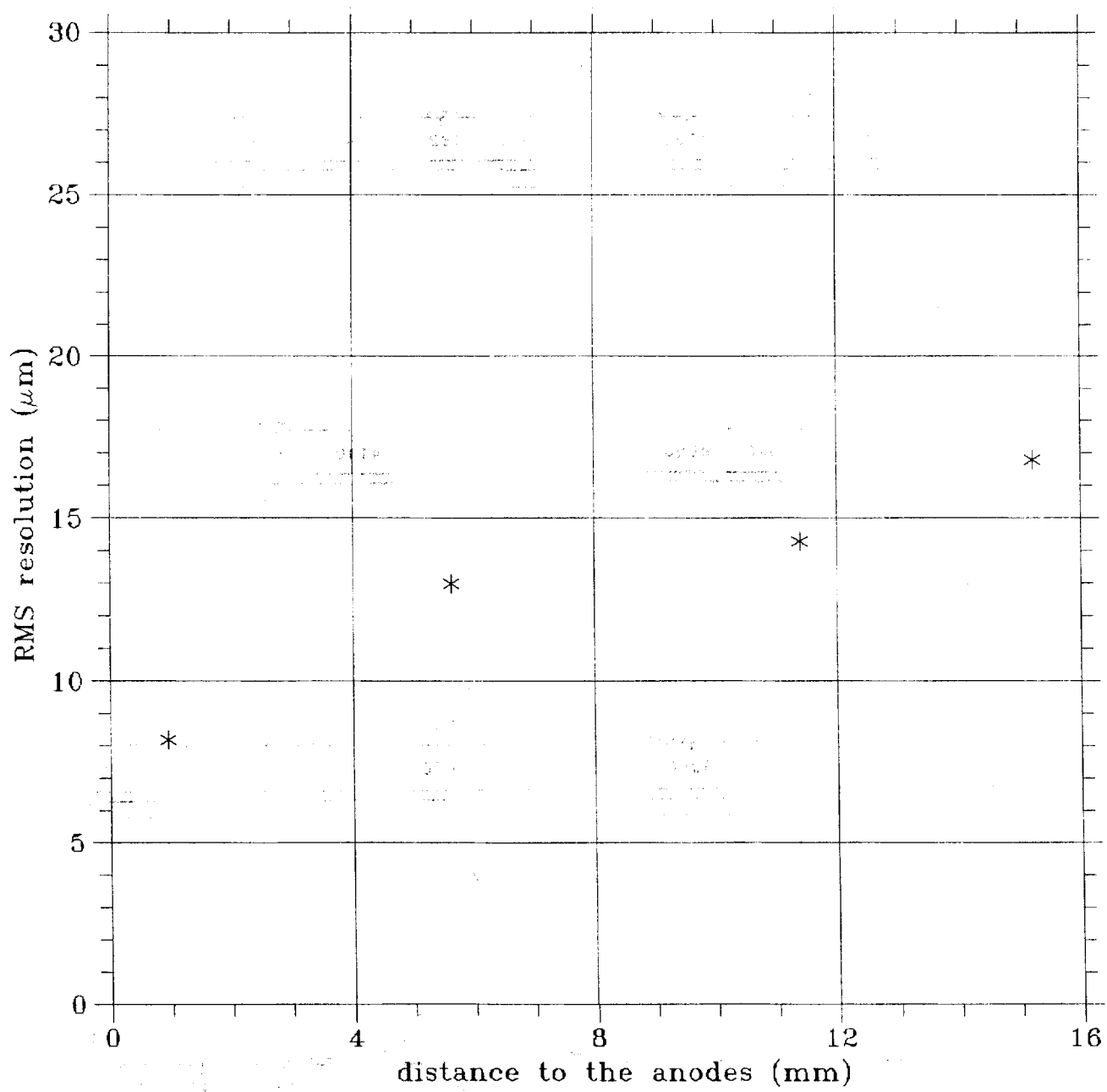
Fig. 9b
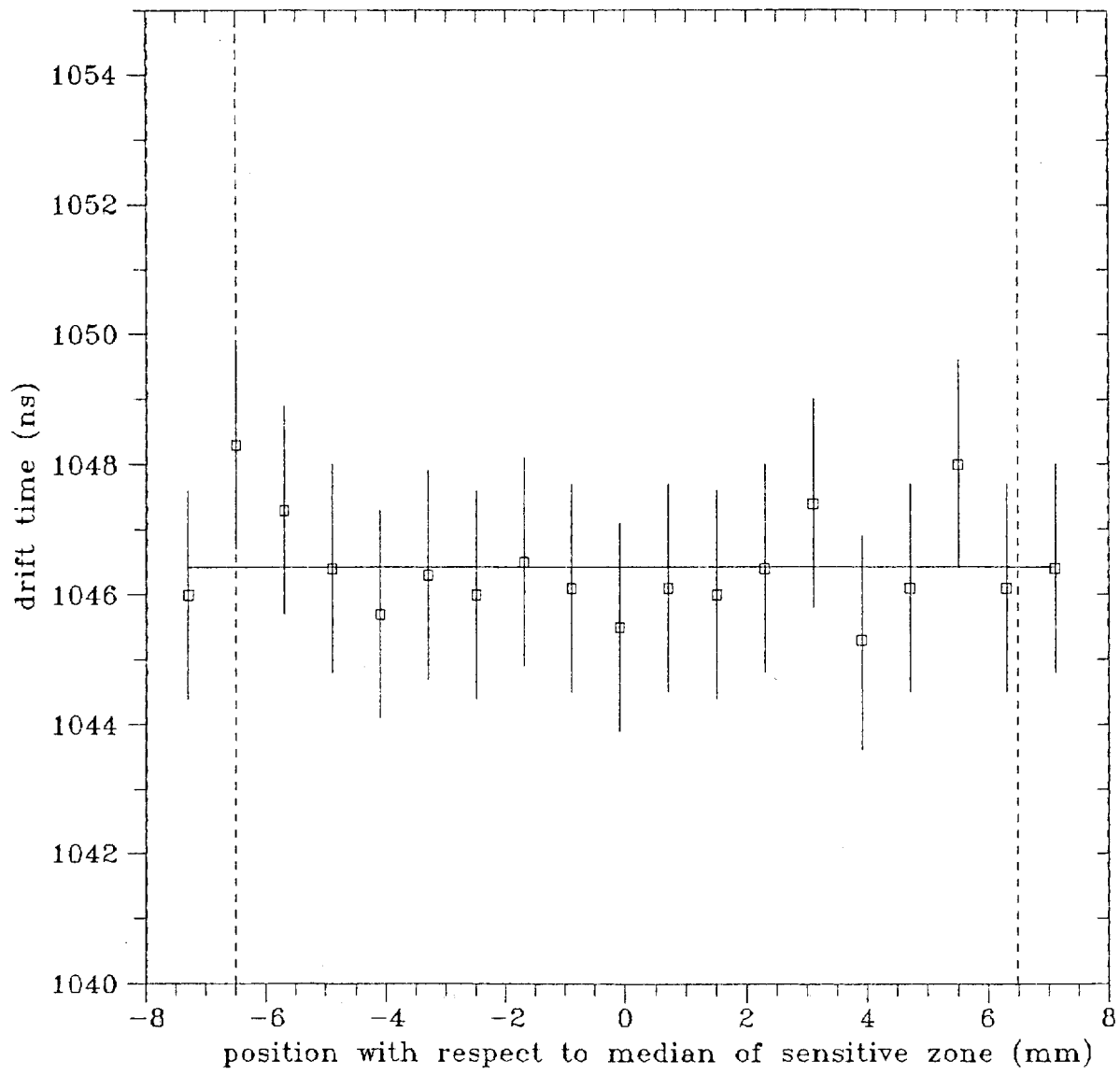
Fig. 10a
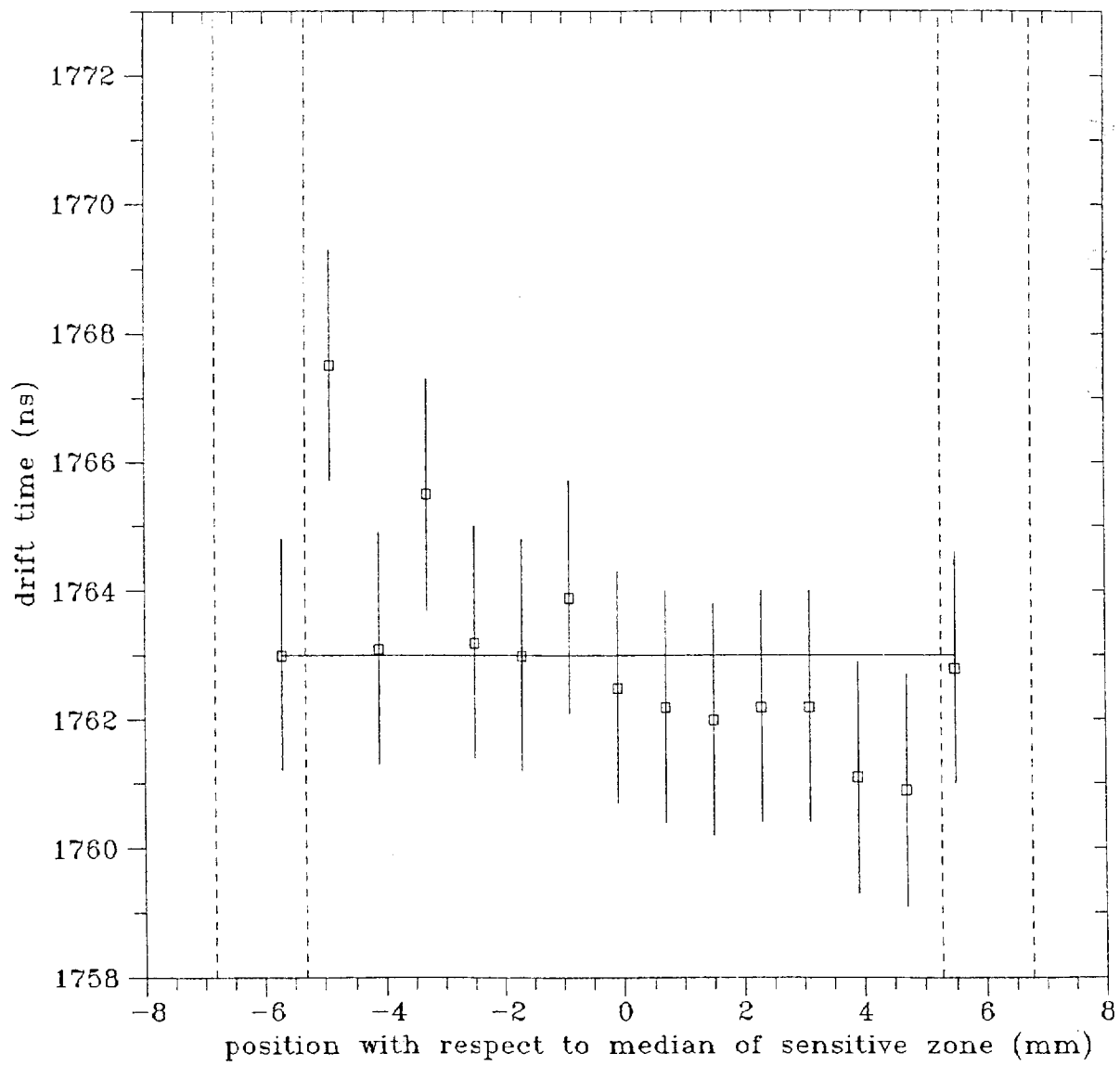
Fig. 10b

Fig. 10c

Fig. 11a

Fig.11b